

Range Image Segmentation by Randomized Region Growing and Bayesian Edge Regularization

¹Smaine Mazouzi and ²Mohamed Batouche

¹Reims University, 816, Evariste Galois, Rue des Crayeres, 51100, Reims, France

²Constantine University, Computer Science Department, 25000, Constantine, Algeria

Abstract: We presented and evaluated a new Bayesian method for range image segmentation. The method proceeds in two stages. First, an initial segmentation was produced by a randomized region growing technique. The produced segmentation was considered as a degraded version of the ideal segmentation, which should be then refined. In the second stage, image pixels not labeled in the first stage were labeled by using a Bayesian estimation, based on some prior assumptions on the regions in the image. Image priors were modeled by a new Markov Random Field (MRF) model. Contrary to most of the authors in range image segmentation, who use only surface smoothness MRF models, our MRF model takes into account also the smoothness of region boundaries. Tests performed with real images from the ABW database show the great potential of the proposed method for significantly improving the segmentation results.

Key words: Image segmentation, range image, randomized region growing, bayesian estimation, markov random field

INTRODUCTION

The segmentation of an image is often necessary to provide a compact and convenient description of its content, suitable for high level image analysis and understanding. It consists in assigning pixels to homogenous and disjoint regions which form a partition of the image. Pixels which belong to the same region share a common propriety, called the region homogeneity criterion. In range images, segmentation methods can be divided into two distinct categories: edge-based segmentation methods and region-based segmentation methods. In the first category, pixels which correspond to discontinuities in depth or in surface normals are selected and chained in order to delimit the regions in the image^[1,2,3]. Edge-based methods are well known for their low computational cost; however, they are very sensitive to noise. On the other hand, region-based methods use geometrical surface features to gather pixels with the same proprieties in disjoint regions^[4,5,6,7]. The region growing technique is widely used. First, region seeds are selected; then regions are enlarged by recursively including homogenous surrounding pixels. Compared to edge-based methods, region-based methods are more stable and less sensitive to noise. However, their efficiency depends strongly on the selection of the region seeds. Some authors have used hybrid approaches. Often a region-based method and an edge-based one are combined so that detected edges are used to initialize and steer a region-based segmentation^[8].

Few authors have integrated Bayesian inference in range image segmentation. Lavalle and Hutchinson^[9] have used a Bayesian test to merge regions in both range and textured images. Region merging is based on some observation vectors and some image priors. The merging of two regions depends on the probability that the resulting region is homogenous. Jain and Nadabar^[10] have proposed a Bayesian method for edge detection in range images. Considering the smoothness of image surfaces as a prior, they use the Line Process (LP) Markov random field (MRF) model^[11] to label image pixels as EDGE or NON-EDGE pixels.

Wang and Wang^[12] have presented a hybrid scheme for range image segmentation. First, they proposed a joint Bayesian estimation of both pixel labels and surface patches. Next, the solution is improved by combining the Scan Line algorithm for edge detection in range images^[3] and the Multi-Level Logistic (MLL) MRF model^[13]. Li^[14] proposed a Markov random field model for surface smoothing with discontinuity preserving in range images. The use of the MAP-MRF (Maximum A Posteriori - Markov Random Field) framework has allowed region smoothing with preserving of both step and roof edges.

In spite of various contributions of the works previously cited, some aspects inherent to range image segmentation were omitted. Indeed, most of the works use Markovian models that are based exclusively on the surface smoothness prior. Moreover, the proposed methods proceed by

assigning pixels to clusters without ensuring the continuity of the resulting clusters. Typically, in the approach proposed by Wang and Wang^[12], the pixels belonging to coplanar regions may be assigned equally to any of these regions. The spatial continuity constraint of resulting regions seems that it was not taken into account.

The method proposed in this study aims first at providing an initial segmentation version, using an improved region growing technique and then to refine this version by a Bayesian-MRF labeling. The refinement of the initial segmentation consists in a Bayesian regularization of unlabeled pixels. The latter are mostly close to region boundaries. A new Markov random field model is used to model the prior information on image regions, by considering both surface and edge smoothness. In the first stage, the image regions are extracted using a randomized region growing technique. The latter consists in a random sampling of region seeds. In the second stage, unlabeled pixels are labeled using a Bayesian estimation, based on two distinct priors. The first one consists of the surface smoothness, which is modeled by the MLL model^[13]. The second one which is introduced through this work consists of the edge smoothness. The new MRF model uses a high-order neighborhood system and is based on the assumption that edge pixels are situated on straight lines that represent region boundaries. The use of the ICM algorithm (Iterated Conditional Modes)^[15] to search for the optimal solution has allowed us to formulate region continuity by defining a constraint on the possible labels of a given pixel. Indeed, the label of a given pixel is selected among the labels corresponding to the regions to which the pixel is close. The experimentations performed with real images from the ABW database^[16] show the great potential of the proposed method to provide an accurate segmentation of range images.

Image segmentation by randomized region seed sampling

Surface modeling: A range image is a discretized two-dimensional array where at each pixel (x,y) is recorded the distance $d_{x,y}$ between the range finder plane and the corresponding point of the scene. Regions in such an image represent the visible patches of object surfaces. To attenuate the white and the impulsive noise contained in the image, a Gaussian filter and a median filter are applied to the raw data. Let d^* a new representation of the row image, where $d^*_{x,y}$ represents the tangent plane to the surface at (x,y) . The best tangent plane at (x,y) is obtained by the multiple regression method using the set of neighboring pixels $\chi(x,y)$. The neighborhood $\chi(x,y)$ is made up of pixels (x',y') situated within a 3×3 window, centred at (x,y) and with close depths

$(d_{x',y'})$ according to a given threshold (Tr_h) . The plane equation in a 3-D coordinate system may be expressed as follows:

$$z=ax+by+c \tag{1}$$

where $(a,b,-1)^T$ is a normal vector to the plane and $|c|/\sqrt{a^2+b^2+1}$ is the orthogonal distance between the plane and the coordinate origin. Parameters a , b and c at (x_0,y_0) are obtained by the minimization of the function Φ , defined as follows:

$$\Phi(a,b,c) = \sum_{(x',y') \in \chi(x_0,y_0)} (ax'+by'+c-d_{x',y'})^2 \tag{2}$$

with $\chi(x,y) = \{(x+i,y+j); (i,j) \in \{-1,0,1\} \wedge |d_{x+i,y+j} - d_{x,y}| < Tr_h\}$

The quality of estimation according to the regression model is also computed:

$$q(x,y) = \sum_{(x',y') \in \chi(x,y)} \frac{(ax+by+c-d_{x',y'})^2}{(d_{x',y'}-d_{x,y})^2} \tag{3}$$

The operations performed on the new image are based on the comparison of two planes. Indeed, we consider that two planes: $z=ax+by+c$ and $z=a'x+b'y+c'$ are equal if they have, according to some thresholds, the same orientation and the same distance to the coordinate origin. Let θ be the angle between the two normal vectors and h the distance between the two planes:

$$\sin(\theta) = \|(a,b,c) \otimes (a',b',c')\| / \sqrt{a^2+b^2+1} \text{ and}$$

$h = |c-c'| / \sqrt{a^2+b^2+1}$. So, the two planes are considered equal if $\sin(\theta) \leq Tr_\theta$ and $h \leq Tr_h$, where Tr_θ and Tr_h are respectively the angle and the distance thresholds. Plane comparison is first used to test if a given pixel belongs to a planar region, given its plane equation. It is also used to test if the pixel is, or is not, a pixel of interest (edge or noise pixel). In this case, the pixel in question is considered as a pixel of interest if at least one of its neighbors has a different plane equation, according to the previous thresholds.

Region growing by randomized region seed sampling:

Inspired from the RANSAC algorithm^[17], our region growing technique is based on random sampling of the region seeds. A generated seed is accepted if only the surface estimation quality q at this seed is greater than a given threshold \underline{Q} . For every accepted seed, a region growing is performed by recursively including homogenous pixels situated on the borders of the region in growth. A given seed centred at (x_i,y_i) is formed by the pixels in a $W \times W$ window, belonging to the same plane. The seed quality is represented by the minimum of estimation qualities of pixels that form the seed. Selection-growing process is repeated until no new region can be created. Random sampling of region seeds allows

to select the best seeds. These latter are characterized by a good quality. It allows to include in a given region the largest possible set of homogenous pixels. Indeed, several seeds within the same region can be generated; however none of these seeds is accepted. The first generated seed for which the quality q is greater than Q will be accepted and considered for region growing. The randomized growing algorithm is described as follows:

```

t=0
Repeat
  Generate a random position (xt,yt)
  If seed quality q>Q then
    Perform a region growing starting from (xt,yt)
  EndIf
  t=t+1
Until none new region was generated since t-dT
// dT is a given time interval; dT>>1
  For each generated region  $R_i$ , the residual
  variance  $\sigma_i^2$  is calculated as follows:

```

$$\sigma_i^2 = \sum_{(x,y) \in R_i} (a_i x + b_i y + c_i - d_{x,y})^2 \quad (4)$$

where (a_i, b_i, c_i) are the plane equation parameters of the region R_i . This parameter will be used in Bayesian edge regularization.

Note that in 2-D images, the variance σ^2 depends only on the noise. Consequently, it is considered constant for all the regions of the image. However, in range images σ^2 depends on both noise and surface orientation, regarding the plane of the range finder. Its value is proportional to the angle of the surface inclination.

Region growing by randomized region seed sampling has provided better results, compared to deterministic region growing (Fig. 1b,c). However, the resulting segmentation often remains unsatisfactory. In Fig. 1c, we can note that most of the unlabeled pixels are those close to region boundaries. We present in the next section a new Bayesian method which allows refining the resulting segmentation by a reliable labeling of unlabeled pixels.

Edge regularization by bayesian inference

MAP-MRF pixel labeling: We have used the piecewise smoothness of image surfaces as well as the piecewise smoothness of region boundaries as priors to model distributions of pixel labels in range images. Let S denote the image lattice. At each site $(x,y) \in S$, $d_{x,y}$ is the depth at the site and $d_{x,y}^*$ represents the corresponding plane equation parameters: $d_{x,y}^* = (a_{x,y}, b_{x,y}, c_{x,y})$.

Let M be the number of regions in the image. So, each site (x,y) can take a label $f_{x,y}$ from the set of labels $L = \{l_1, \dots, l_M\}$. The labeling set $F = \{f_{x,y}, (x,y) \in S, f_{x,y} \in L\}$, represents a segmentation of the image. If we assume that F is Markovian, segmenting S according

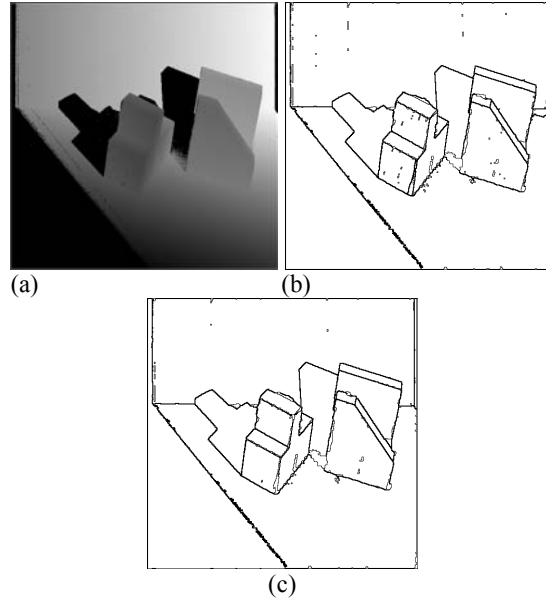


Fig. 1: Region growing. (a) Range image (abw.test.6); (b) Segmentation result by a deterministic region growing; (c) Segmentation result by a randomized region growing

to the MAP-MRF framework^[18] is equivalent to calculate the maximum a posteriori (MAP) of the distribution of the set F : $P(F/d)$, by considering F as a Markov Random Field (MRF).

According to Bayes' rule, the maximum a posteriori $P(F/d)$ is expressed as follows:

$$P(F/d) = \frac{p(d/F)P(F)}{p(d)} \quad (5)$$

$P(F) = Z^{-1} e^{-U(F)}$ is the a priori probability of F obtained according to the Markov-Gibbs equivalence theorem^[19]. $Z = \sum_F e^{-U(F)}$ is a normalization constant called the partition function.

The a priori energy $U(F)$ is a sum of clique potentials $V_c(F)$ over the set of all possible cliques C : $U(F) = \sum_{c \in C} V_c(F)$.

In our MRF model we have considered two sets of cliques: the set C_1 of cliques, formed by two neighboring sites according to the 4-neighborhood system and the set C_2 of cliques, formed by 9 sites located in a 3×3 window. By using the parameter ζ , ($\zeta < 0$), the potential V^1 of cliques in C_1 is defined as follows:

$$V^1(f_{x,y}, f_{x',y'}) = \begin{cases} 0 & \text{if } f_{x,y} = f_{x',y'} \\ -\zeta & \text{otherwise} \end{cases} \quad (6)$$

In order to define the potential V^2 of cliques in blocks of 3×3 sites, we use the following notations: let c_9 be a clique of 3×3 sites centred at (x,y) :

$$c_9(x,y) = \left\{ f_{x+i,y+j}; (i,j) \in \{-1,0,+1\} \right\} \quad (7)$$

Let's define the transformation Γ , defining the order of sites in cliques of C_2 ; $\Gamma : C_2 \rightarrow F^9$, so that:

$$\Gamma(c_9(x, y)) = (f_{x-1, y-1}, \dots, f_{x+1, y+1}) \quad (8)$$

By using the parameter κ , ($\kappa < 0$) and considering possible configurations of cliques in C_2 (Fig. 2) the potential V^2 can thus be expressed as follows:

$$V^2(\Gamma(c_9(x, y))) = \begin{cases} \kappa & \text{if } \exists(x, y), (x', y'), (x'', y'') \mid \\ & f_{x, y} = f_{x', y'} = f_{x'', y''} \wedge \\ & \phi((x', y'), (x, y), (x'', y'')) = \pi \\ \\ 0 & \text{if } \exists(x, y), (x', y'), (x'', y'') \mid \\ & f_{x, y} = f_{x', y'} = f_{x'', y''} \wedge \\ & \phi((x', y'), (x, y), (x'', y'')) = \frac{2\pi}{3} \\ \\ -\kappa & \text{otherwise} \end{cases} \quad (9)$$

Where $\phi((x', y'), (x, y), (x'', y''))$ is the angle between the two vectors $(x'-x, y'-y)^T$ and $(x''-x, y''-y)^T$.

The potential V^1 models surface smoothness, whereas V^2 models edge smoothness. Configurations used to define V^2 depend on the surface type. For images containing polyhedral objects, considered in this work, V^2 is defined on the basis that the boundary between two adjacent regions is formed by pixels belonging to the same straight line (Fig. 2). So, configurations which correspond to locally unsmoothed edges are penalized by using a positive clique potential ($-\kappa$).

The likelihood distribution $p(d/F)$, is obtained by assuming that the observations d are degraded by an independent Gaussian noise:

$$d_{x, y} = a_{f_{x, y}} x + b_{f_{x, y}} y + c_{f_{x, y}} + e(x, y) \quad (10)$$

with $e(x, y) \sim N(0, \sigma_{f_{x, y}}^2)$.

So, the likelihood distribution is expressed as follows:

$$p(d/F) = \frac{1}{\prod_{(x, y) \in S} \sqrt{2\pi\sigma_{f_{x, y}}^2}} e^{-U(d/F)} \quad (11)$$

with the likelihood energy $U(d/F)$ defined by:

$$U(d/F) = \sum_{(x, y) \in S} \frac{(a_{f_{x, y}} x + b_{f_{x, y}} y + c_{f_{x, y}} - d_{x, y})^2}{2\sigma_{f_{x, y}}^2} \quad (12)$$

Since $p(d)$ is constant for a fixed d , the solution F^* is obtained by maximizing the a posteriori probability $P(F/d) \propto p(d/F)P(F)$, which is equivalent to minimizing the a posteriori energy $U(F/d) = U(d/F) + U(F)$:

$$F^* = \arg \max_F (U(d/F) + U(F)) \quad (13)$$

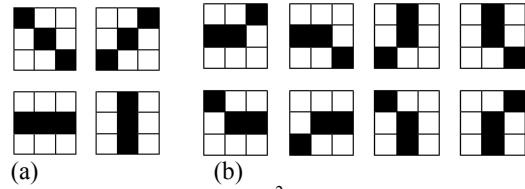


Fig. 2: Clique potential $V^2(c_9)$ defined according to the edge smoothness prior. (a) Full locally smooth edge: $V^2(c_9)=\kappa$; (b) Partial locally smooth edge: $V^2(c_9)=0$; Otherwise, the edge is not locally smooth: $V^2(c_9)=-\kappa$

Computation of the optimal solution: By assuming that F is Markovian and the observations $\{d_{x, y}\}$ are conditionally independent, we have used the ICM algorithm to minimize the a posteriori energy $U(F/d)$. By considering $U(F/d)$ as a sum of energies over all image sites: $U(F/d) = \sum_{(x, y) \in S} U(f_{x, y}/d_{x, y})$, we can separate it in two terms:

$$U(F/d) = \sum_{(x, y) \in S'} U(f_{x, y}/d_{x, y}) + \sum_{(x, y) \in S-S'} U(f_{x, y}/d_{x, y}) \quad (14)$$

where S' is the set of sites which have not been labeled in the first stage (by region growing): $S' = \{(x, y) \in S \mid f_{x, y} \text{ is undefined}\}$. Assuming the correctness of the labeling of the set $S-S'$ (performed in the first stage), the term $\sum_{(x, y) \in S-S'} U(f_{x, y}/d_{x, y})$ is thus constant.

Minimizing the energy $U(F/d)$ is equivalent to minimizing the energy $U'(F/d)$ which corresponds to the sites in S' : $U'(F/d) = \sum_{(x, y) \in S'} U(f_{x, y}/d_{x, y})$ (15)

The assumption of the correctness of the labeling of $S-S'$ allows also to define a constraint on the set of possible values that a site in S' can have during the execution of the ICM algorithm. Indeed, the label $f_{x, y}^k$ at the iteration k , of a site (x, y) is chosen among the set $L'(x, y) \subset L$ containing the labels of the sites, labeled in the first stage and located in a $W \times W$ window centred at (x, y) . Formally, $L'(x, y)$ is defined as follows:

$$L'(x, y) = \left\{ l \mid \exists(x', y') \in S-S', (x-x', y-y') \in [-W/2, W/2]^2 \wedge f_{x', y'} = l \right\} \quad (16)$$

The two previous heuristics allow to speed up the calculation of the minimum of the a posteriori energy $U'(F/d)$. They allow also to satisfy the region continuity constraint. For the latter problem, if we assume that the distance between two coplanar regions R and R' is greater than W , the labels l_R and $l_{R'}$ corresponding respectively to R and R' , cannot belong to the same set $L'(x, y)$. For example, if the site (x, y) belongs to R , it can not be labeled $l_{R'}$, although energies $U'(l_R/d_{x, y})$ and $U'(l_{R'}/d_{x, y})$ are equal.

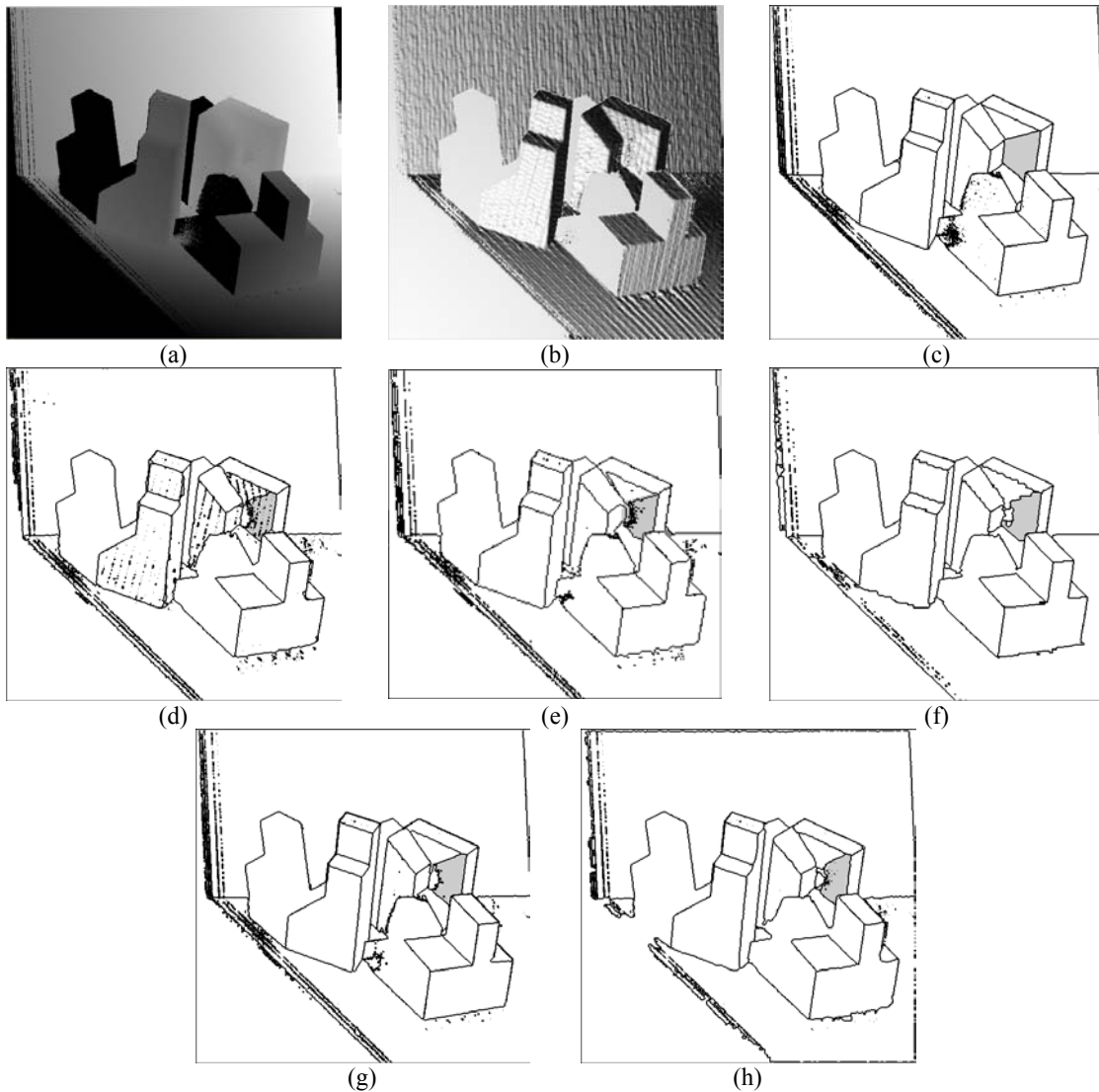


Fig. 3: Segmentation results of abw.test.8 image. (a) Range image; (b) Redered image; (c) Ground truth segmentation (GT); (d) USF result; (e) WSU result; (f) UB result; (g) UE result; (h) BRIS result

RESULTS

Evaluation framework: Hoover *et al.* have proposed a dedicated framework for the evaluation of range image segmentation algorithms^[16], which has been used in several related works^[3,20,7,6,4]. The framework consists of a set of real range images and a set of objective performance metrics. It allows to compare a machine-generated segmentation (MS) with a manually-generated segmentation, supposed ideal and representing the ground truth (GT). The most important performance metrics are the numbers of instances respectively of correctly detected regions, over-segmented regions, under-segmented regions,

missed regions and noise regions. Region classification is performed according to a compare tool tolerance T ; $50% < T \leq 100%$, which reflects the strictness of the classification. The 40 real images of the ABW database are divided into two subsets: 10 training images and 30 test images. The training images are used to estimate the parameters of a given segmentation method. Using these parameters, the method is applied to the test images. The Performance metrics are computed and stored in order to be used to compare the involved methods. In our case, four methods, namely USF, WSU, UB and UE, cited in ^[16] are involved in the comparative study.

Parameter selection: Since the evaluation framework provides a set of training images with ground truth segmentation (GT), we have opted for a supervised approach for the estimation of parameters. For the proposed method, named BRIS for Bayesian Range Image Segmentation, six parameters should be fixed: Tr_θ , Tr_h , W , Q , ζ and κ . The performance criterion used in parameter selection is the average number of correctly detected regions with the compare tool tolerance T set to 80%. The parameters are divided into two subsets: 1) Tr_θ , Tr_h , W and Q which represent respectively the angle threshold, the depth threshold, the window size and the seed quality threshold. These parameters are used by the randomized region growing algorithm. 2) Parameters ζ and κ express respectively the clique potentials V^1 and V^2 . These two parameters are used in the segmentation refinement.

For the first parameter subset: Tr_θ , Tr_h , W and Q , 256 combinations namely $(Tr_\theta, Tr_h, W, Q) \in \{15^\circ, 18^\circ, 21^\circ, 24^\circ\} \times \{12, 16, 20, 24\} \times \{5, 7, 9, 11\} \times \{0.90, 0.95, 0.97, 0.99\}$, were run on the training images. The threshold Tr_θ was set to 21° . Note that higher values of this parameter under-differentiate regions regarding their orientations and lead to an under-segmentation of the image. However, lower values over-differentiate regions and lead to an over-segmentation. It results in a high number of false and small regions, which should be merged in the true neighboring regions. The threshold Tr_h is set to 16. Values significantly greater than 16 can lead to inappropriate merging of some parallel overlapped regions. However, if Tr_h is significantly less than 16, highly sloping surfaces can not be detected as planar regions^[3]. This results in a high rate of missed regions. Parameters W and Q were set respectively to 7 and 0.97. The selected value of W permits to estimate the plane equation by considering a wide neighborhood (W^2 pixels), whereas Q ensure that the plane parameters are reliable and the window $W \times W$ is not located between two different regions.

We have used the Coding method^[19] to estimate the parameters ζ and κ . For each image in the training set, a pair of values of these parameters is calculated. The two averages are then used as the parameter values. We have used a single Coding of the set $S-S'$. It corresponds to the cliques of 3×3 sites. Indeed, we assume that the regularization of the region boundaries is more convenient for the labeling of unlabeled pixels, because these pixels are mostly close to the region boundaries. The optimal values for each training image is calculated by the simulated annealing algorithm^[21], using a Gibbs sampler^[11]. The average values of ζ and κ obtained with the training set were respectively -0.373×10^{-5} and -0.587×10^{-4} .

Figure 3 shows the segmentation results of the image *abw.test.8*, with the compare tool tolerance T set to 80%. This image was considered as a typical image to compare the involved methods^[16,6]. Figure 3a, 3b and 3c show respectively the range image, the rendered image and the ground truth segmentation (GT). Figure 3d, 3e, 3f and 3g are segmentation results obtained respectively by USF, WSU, UB and UE methods. Figure 3h presents the segmentation result obtained by our method.

Metrics in Table 1 show that all image regions detected by the best-referenced segmenter (UE) were detected by our method. Except the shadowed region, where all methods fail to detect, all object regions were detected. The incorrectly detected regions are those with small sizes and situated on the horizontal support. Compared to the other methods, values of incorrect detection metrics are also good. Our method is equivalent to UE and scored higher than the others.

Table 1: Comparison results with *abw.test.8* image for $T=80\%$

Method	GT Region	Correct detect.	Over-segm.	Under-segm.	Miseed	Noise.
USF	21	17	0	0	4	3
WSU	21	12	1	1	6	4
UB	21	16	2	0	3	6
UE	21	18	1	0	2	2
BRIS	21	18	2	0	1	1

Table 2: Average results of the different involved methods for $T=80\%$

Method	GT Region	Correct detec.	Over-segm.	Under-segm.	Miseed	Noise.
USF	15.2	12.7	0.2	0.1	2.1	1.2
WSU	15.2	9.7	0.5	0.2	4.5	2.2
UB	15.2	12.8	0.5	0.1	1.7	2.1
UE	15.2	13.4	0.4	0.2	1.1	0.8
BRIS	15.2	13.1	0.4	0.1	1.7	0.9

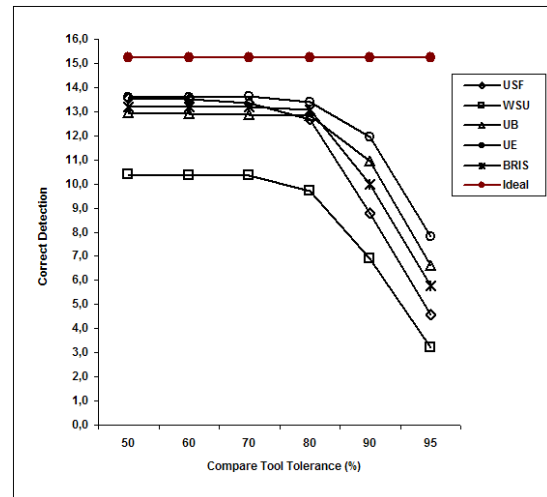


Fig. 4: Average results of correctly detected regions of all methods, according to the compare tool tolerance T ; $50\% < T \leq 100\%$

Table 2 shows the average results obtained with all test images and for all performance metrics. The compare tool tolerance was set to the typical value 80%. By considering both correct detection and incorrect detection metrics, obtained results show a very good efficiency of our method.

Figure 4 shows the average numbers of correctly detected regions for all test images and according to the compare tool tolerance T ; $T \in \{51, 60, 70, 80, 90$ and 95% .

Results show that the number of correctly detected regions by our method is in average better than those of USF, UB and WSU. For instance, our system scored higher than WSU for all the values of the compare tool tolerance T . It scored higher than USF for $T \in \{80\%, 90\%, 95\%\}$ and better than UB for $T \in \{50, 60, 70$ and $80\%\}$. For all incorrect detection metrics (Over-segmentation, Under-segmentation, Missed, Noise), our method has equivalent scores to those of UE and USF. The two latter scored higher than UB and WSU.

CONCLUSION

We have presented in this paper a new Bayesian method for range image segmentation. Region growing by randomized seed sampling, introduced in this work provides an initial degraded segmentation. Results at this stage are better than those obtained with deterministic region growing. The refinement of the initial segmentation using the MAP-MRF framework has allowed improving significantly the segmentation results. We have presented a new MRF model which allows to model both surface and edge smoothness, considered as prior assumptions on regions in range images.

Extensive tests were performed on real images from the ABW database. Obtained results show the great potential of the proposed method for providing an efficient and accurate range image segmentation. The proposed method can be extended to curved objects, by defining the surface proprieties specific to these objects, as well as the appropriate MRF models.

REFERENCES

1. Inokuchi, S., T. Nita, F. Matsuda and Y. Sakurai, 1982. A three dimensional edge-region operator for range pictures. In 6th International Conference on Pattern Recognition, pp: 918–920.
2. Fan, T.J., G.G. Medioni and R. Nevatia, 1987. Segmented description of 3-D surfaces. IEEE J. Robotics Automat, 3: 527–538.

3. Jiang, X. and H. Bunke, 1999. Edge detection in range images based on Scan Line approximation. Computer Vision and Image Understanding, 73: 183–199.
4. Bab Hadiashar, A. and N. Gheissari,, 2006. Range image segmentation using surface selection criterion. IEEE Transactions on Image Processing, 15 :2006–2018.
5. Kang, S.B. and K. Ikeuchi, 1993. The complex EGI: A new representation for 3-D pose determination. IEEE Transactions on Pattern Analysis and Machine Intelligence, 15: 707–721.
6. Ding, Y., X. Ping, M. Hu and D. Wang, 2005. Range image segmentation based on Randomized Hough Transform. Pattern Recognition Letters, 26: 2033–2041.
7. Li, S. and D. Zhao, 2003. Gradient-based polyhedral segmentation for range images. Pattern Recognition Letters, 24: 2069–2077.
8. Lim, A.W.T., E.K. Teoh and D.P. Mital, 1994. A hybrid method for range image segmentation. J. Mathematical Imaging and Vision, 4: 69–80.
9. LaValle, S. M. and S. A. Hutchinson, 1993. Bayesian region merging probability for parametric image models. In Proc. IEEE Conference on Computer Vision and Pattern Recognition, pp: 778–779.
10. Jain, A.K. and S.G. Nadabar, 1990. MRF model-based segmentation of range images. International Conference on Computer Vision, pp: 667–671.
11. Geman, S. and D. Geman, 1984. Stochastic relaxation, Gibbs distributions and the Bayesian restoration of images. IEEE Transactions on Pattern Analysis and Machine Intelligence, 6: 721–741.
12. Wang, X. and H. Wang, 2004. Markov Random Field modeled range image segmentation. Pattern Recognition Letters. 25: 367–375.
13. Derin, H. and H. Elliott, 1987. Modeling and segmentation of noisy and textured image using Gibbs Random Fields. IEEE Trans. Pattern Analysis and Machine Intelligence, 9: 39–55.
14. Li, S. Z., 2000. Roof-edge preserving image smoothing based on MRFs. IEEE Transactions on Image Processing, 9:1134–1138.
15. Besag, J.E., 1986. On the statistical analysis of dirty pictures. J. Royal Stat. Soc., Series B, 48: 259–302.
16. Hoover, A., G. Jean-Baptiste, X. Jiang, P. J. Flynn, H. Bunke, D. B. Goldgof, K. W. Bowyer, D. W. Eggert, A. W. Fitzgibbon and R. B. Fisher, 1996. An experimental comparison of range image segmentation algorithms. IEEE Trans. on Pattern Analysis and Machine Intelligence, 18: 673–689.

17. Fischler, M. A. and R. C. Bolles, 1987. Random sample consensus: a paradigm for model fitting with applications to image analysis and automated cartography., pp: 726–740.
18. Li, S. Z., 2001. Markov Random Field modeling in image analysis. Springer-Verlag New York, Inc., Secaucus, NJ, U.S.A.
19. Besag, J.E., 1974. Spatial interaction and statistical analysis of lattice systems. *J. Royal Statistical Society, Series B*, 36: 192–236.
20. Jiang, X., K. W. Bowyer, K. W. Morioka, K. W. Hiura, K. Sato, S. Inokuchi, M. Bock, C. Guerra, R. E. Loke and J. M. Hans du Buf, 2000. Some further results of experimental comparison of range image segmentation algorithms. *Intl. Conf. Pattern Recognition*, pp: 4877–4882.
21. Kirkpatrick, S., C. D. Gelatt, Jr. and M. P. Vecchi, 1987. Optimization by simulated annealing. *Readings in computer vision: issues, problems, principles and paradigms*, pp: 606–615.